Evidence for rRNA 2′-O-methylation plasticity: Control of intrinsic translational capabilities of human ribosomes

Jenny Erales[a,b], Virginie Marchand[c], Baptiste Panthu[b,d,e], Sandra Gillot[f], Stéphane Belin[a,b,1], Sandra E. Ghayad[a,b,2], Maxime Garcia[a,b], Florian Laforêts[a,b], Virginie Marcel[a,b], Agnès Baudin-Baillieu[f], Pierre Bertin[f], Yohann Couté[g], Annie Adrait[g], Mélanie Meyer[h], Gabriel Therizols[a,b,3], Marat Yusupov[i], Olivier Namy[f], Théophile Ohlmann[b,d,e], Yuri Motorin[i], Frédéric Catez[a,b,4,5], and Jean-Jacques Diaz[a,b,4,5]

[a]Centre de Recherche en Cancérologie de Lyon, UMR, INSERM 1052, CNRS 5286, Centre Léon Bérard, F-69373 Lyon, France; [b]Institut des Sciences Pharmaceutiques et Biologiques, Université de Lyon, F-69003 Lyon, France; [c]Next-Generation Sequencing Core Facility, FR3209 Bioingénierie Moléculaire Cellulaire et Thérapeutique, CNRS, Lorraine University, F-54505 Vandoeuvre-les-Nancy, France; [d]Centre International de Recherche en Infectiologie, Université de Lyon, 69364 Lyon, France; [e]Ecole Normale Supérieure de Lyon, 69342 Lyon, France; [f]Institute for Integrative Biology of the Cell, Commissariat à l'Energie Atomique, CNRS, Université Paris-Sud, Université Paris-Saclay, 91190 Gif-sur-Yvette, France; [g]Laboratoire Biologie à Grande Échelle, Institut de Biosciences et Biotechnologies de Grenoble, Université Grenoble Alpes, Commissariat à l'énergie Atomique et aux Énergies Alternatives, INSERM, 38000 Grenoble, France; [h]Institut de Génétique et de Biologie Moléculaire et Cellulaire, CNRS UMR 7104 INSERM U 964, F-67404 Illkirch, France; and [i]Ingénierie Moléculaire et Physiopathologie Articulaire, UMR7365, CNRS, Université de Lorraine, F-54505 Vandoeuvre-les-Nancy, France

Edited by Ada Yonath, Weizmann Institute of Science, Rehovot, Israel, and approved October 31, 2017 (received for review May 9, 2017)

Ribosomal RNAs (rRNAs) are main effectors of messenger RNA (mRNA) decoding, peptide-bond formation, and ribosome dynamics during translation. Ribose 2′-O-methylation (2′-O-Me) is the most abundant rRNA chemical modification, and displays a complex pattern in rRNA. 2′-O-Me was shown to be essential for accurate and efficient protein synthesis in eukaryotic cells. However, whether rRNA 2′-O-Me is an adjustable feature of the human ribosome and a means of regulating ribosome function remains to be determined. Here we challenged rRNA 2′-O-Me globally by inhibiting the rRNA methyl-transferase fibrillarin in human cells. Using RiboMethSeq, a nonbiased quantitative mapping of 2′-O-Me, we identified a repertoire of 2′-O-Me sites subjected to variation and demonstrate that functional domains of ribosomes are targets of 2′-O-Me plasticity. Using the cricket paralysis virus internal ribosome entry site element, coupled to in vitro translation, we show that the intrinsic capability of ribosomes to translate mRNAs is modulated through a 2′-O-Me pattern and not by nonribosomal actors of the translational machinery. Our data establish rRNA 2′-O-Me plasticity as a mechanism providing functional specificity to human ribosomes.

2′-O-methylation | fibrillarin | ribosomal RNA | translational control | RNA epigenetics

Translational control is one of the most important regulators of gene expression (1). Translation is regulated through different mechanisms and coordinated with cell signaling. The best-described translational regulation pathways operate through nonribosomal elements, such as the messenger RNA (mRNA) sequence and modification, canonical translation factors, transfer RNAs (tRNAs), micro RNAs (miRNAs), and RNA binding proteins (2, 3). Recently, several studies have provided compelling evidence that regulation of ribosomal proteins or ribosome biogenesis factors was associated with selective regulation of mRNA subsets (4–7). These observations led to the hypothesis of a ribosome-mediated translational control through functionally "specialized ribosomes." However, direct molecular evidence that ribosomes displaying a different ribosomal RNA (rRNA) or protein composition carry different translational capabilities remains to be provided to validate the concept of specialized ribosomes.

In eukaryotes, rRNAs undergo 12 different types of chemical modification, on at least 112 (of 5,475 nt) and 212 (of 7,184 nt) nucleotides in yeast and human, respectively (8). However, despite being one of the best-characterized, the role of the rRNA epitranscriptome remains largely unknown. Among the different types of chemical modifications, 2′-O-methylation (2′-O-Me) is the most abundant modification of eukaryotic rRNA, with 55 and 106 sites mapped in yeast and in human rRNA, respectively (9, 10). In human rRNA, 2′-O-Me is carried out by the methyl transferase fibrillarin (FBL) associated with the

Significance

Translational control is a cornerstone of gene-expression regulation in physiological and pathological contexts. The contribution of nonribosomal factors, including messenger RNAs (mRNAs) and mRNA-bound factors, to translational control have been extensively studied. Recently, the hypothesis of a ribosome-mediated regulation emerged, which proposes that cells produce ribosomes of different composition and displaying different translational properties. This work reveals that ribosomal RNA 2′-O-methylation can be modulated in human ribosomes, including at key functional sites for translation, and that changes in the 2′-O-methylation pattern control the intrinsic capabilities of ribosomes to translate mRNAs. This work directly demonstrates the existence of composition-modified ribosomes and their associated change in translational activity as conceptualized by the specialized ribosome concept.

Author contributions: M.Y., O.N., T.O., Y.M., F.C., and J.-J.D. designed research; J.E., V. Marchand, B.P., S.G., S.B., S.E.G., M.G., F.L., V. Marcel, A.B.-B., Y.C., A.A., and F.C. performed research; M.M., G.T., M.Y., T.O., and Y.M. contributed new reagents/analytic tools; J.E., V. Marchand, B.P., S.B., S.E.G., P.B., Y.C., O.N., Y.M., F.C., and J.-J.D. analyzed data; J.E. and M.M. performed structural analysis; and J.E., V. Marchand, B.P., F.C., and J.-J.D. wrote the paper.

The authors declare no conflict of interest.

This article is a PNAS Direct Submission.

Data deposition: The mass spectrometry proteomics data have been deposited in the ProteomeXchange Consortium via the PRIDE partner repository (accession no. PXD00724). RNA-Seq data of RiboMethSeq data have been deposited in the European Nucleotide Archive database (accession no. PRJEB43738). The RNA-Seq data of Ribosome Profiling have been deposited in the Gene Expression Omnibus (GEO) database, https://www.ncbi.nlm.nih.gov/geo (accession no. GSE105248).

[1]Present address: Grenoble Institut des Neurosciences, University of Grenoble Alpes, F-38000 Grenoble, France.

[2]Present address: Department of Biology, Faculty of Science II, Lebanese University, Jdeidet, Lebanon.

[3]Present address: Department of Urology, University of California, San Francisco, CA 94158.

[4]F.C. and J.-J.D. contributed equally to this work.

[5]To whom correspondence may be addressed. Email: frederic.catez@lyon.unicancer.fr or jean-jacques.diaz@lyon.unicancer.fr.

This article contains supporting information online at www.pnas.org/lookup/suppl/doi:10.1073/pnas.1707674114/-/DCSupplemental.

RNA-binding protein 15.5kDa and the core proteins NOP56 and NOP58. Methylation at each site is guided by small nucleolar RNAs (snoRNAs) from the C/D box snoRNA family, which carry a complementary sequence to the target rRNA.

A significant amount of data supports an essential role for rRNA 2′-O-Me in ribosomal activity. About 70% of 2′-O-Me sites are conserved from yeast to human, particularly those located within functional regions of rRNAs (11). Studies using snoRNA knockout yeast strains revealed the importance of 2′-O-Me for the molecular functioning of ribosomes and for cell fitness, and their potential impact on rRNA folding. In yeast, inhibition of 2′-O-Me at several positions was required to severely impair translation and cell growth (12, 13). In contrast, inhibition of 2′-O-Me at single sites in zebrafish was sufficient to induce embryonic lethality, indicating that the role of individual 2′-O-Me is dependent on the cellular context (14). Finally, dysregulations in C/D box snoRNA gene expression have been linked to human diseases, including cancer or inherited genetic disorders, such as the Prader-Willy syndrome (15). The mechanisms by which C/D box snoRNAs adversely impact human cell behavior remain to be determined, and a link with their 2′-O-Me guiding activity and ribosomal function needs to be established, since an impact of snoRNAs on other cellular functions cannot be excluded. *FBL* (encoded by *NOP1* in yeast) is essential for rRNA 2′-O-Me in yeast and crucial for proper mouse development (16, 17). In addition, in yeast and mammals, FBL participates in pre-rRNA cleavage by association with C/D box snoRNAs, such as U3 or U14 (18), and regulates RNA *Pol I* activity on rDNA gene promoters by methylating a glutamine residue of histone H2A, by an unknown mechanism (19). *FBL* expression was recently shown to be highly modulated in physiological and pathological contexts, such as development (20), stem cell differentiation (21), viral infection (17), and cancer (7, 22). In cellular models of cancer, forced *FBL* up- or down-regulation modulated tumor progression (7). In addition, maintained expression of *FBL* in mouse embryonic stem cells prolonged their pluripotent state (21). In breast cancer cells, changes in *FBL* expression were correlated with alterations in the level of rRNA 2′-O-Me, with alterations in translational accuracy and with efficient translational initiation of mRNAs containing internal ribosome entry site (IRES) elements (7, 22, 23). However, due to the different activities of FBL, more data are needed to demonstrate that the effect of FBL modulation on translational activity is due to its impact on 2′-O-Me.

While the functional importance of 2′-O-Me is supported by genetic, developmental, cellular, and structural studies, whether the 2′-O-Me pattern represents an adjustable feature of ribosomes and a molecular basis of ribosome regulation is not yet determined. Initial proof supporting that 2′-O-Me could be modulated was provided in cellular models of breast cancer and in thalassemia patients using site-by-site analyses (7, 24, 25). However, a comprehensive view of 2′-O-Me within the four rRNAs, as well as a quantitative evaluation of the level of methylation at each site, is still missing. In the present study, we extensively characterize ribosomes following *FBL* down-regulation in HeLa cells. Using the recently developed RiboMethSeq approach, we show that the rRNA 2′-O-Me pattern can be qualitatively and quantitatively modulated. Mapping of the position of methylated nucleotides and their methylation frequency on the 3D structure of the human ribosome revealed an unsuspected 2′-O-Me plasticity within the critical functional domains of the ribosome, responsible for the ribosome translational activity. Using IRES-containing mRNAs as models coupled to hybrid in vitro translation assays, we demonstrate that the intrinsic capability of ribosomes to translate mRNAs is directly controlled by 2′-O-Me. Taken together, these studies establish rRNA 2′-O-Me and its plasticity as a molecular mechanism to regulate the translational activity of ribosomes.

Results

***FBL* Knockdown Decreases Ribosome Biogenesis and Global rRNA 2′-O-Me in Human Cells.** With the aim of altering global rRNA 2′-O-Me, we inhibited *FBL* expression in HeLa cells using small interfering RNA (siRNA). Transfection conditions were set up to obtain a 5- to 10-fold *FBL* knockdown over a period of 5 d to enable ribosome turnover (Fig. S1*A*). The decrease in FBL did not induce a widespread disorganization of nucleoli or instability of major nucleolar proteins (Fig. S1 *B* and *C*). *FBL* knockdown induced a clear, yet incomplete inhibition of the processing of the 5′-ETS region of the pre-rRNA, consequently inhibiting 18S rRNA maturation (Fig. S1*D*), an observation in agreement with previous studies on yeast *NOP1* and with the association of FBL with C/D box snoRNAs involved in pre-rRNA folding and cleavage (18). In contrast, the processing of 5.8S and 28S rRNAs was not affected by *FBL* knockdown. Consistently, ribosome biogenesis was sufficient to maintain ribosome production at ∼80% of that of control cells (Fig. S1*E*). Since FBL participates in rRNA processing (Fig. S1*D*), we speculated that *FBL* knockdown could alter the assembly of ribosomal proteins (RPs). The assembly of newly synthesized ribosomal subunits appeared similar in *FBL* knockdown and control cells as evaluated using 2D-PAGE on ribosomes purified from isotope pulse-labeled cells (Fig. S1*F*). This observation was strengthened by label-free quantitative proteomics analysis, which showed no significant difference between ribosomes extracted from *FBL* knockdown cells compared with control cells (Fig. 1*A* and Dataset S1). Taken together, these findings indicate that FBL does not control the final stoichiometry of proteins in cytoplasmic ribosomes.

Next, we investigated the impact of a decrease in FBL on levels of rRNA 2′-O-Me. Because 2′-O-Me was shown to be an early and primarily cotranscriptional event (26, 27), we first analyzed methylation of the pre-rRNA by pulse labeling (Fig. 1*B*). *FBL* knockdown induced a 33.8% (±19.2, $P = 0.064$) decrease in the level of pre-rRNA methylation. Thus, as could be anticipated, knockdown of the rRNA methyl-transferase fibrillarin induced a global decrease in methylation of the pre-rRNA.

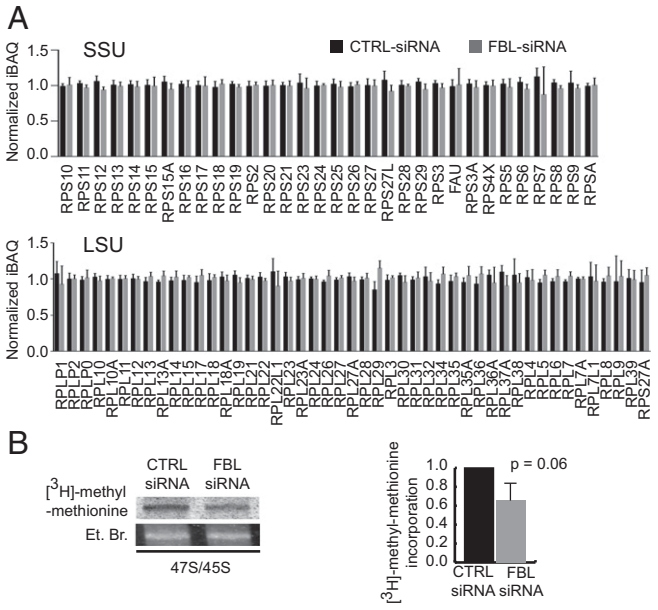

Fig. 1. *FBL* knockdown impacts rRNA 2′-O-Me and not ribosome protein composition in human cells. (*A*) Label-free quantitative proteomic analysis of 0.5 M KCl-purified cytoplasmic ribosomes from siRNA transfected cells. Normalized Intensity-based absolute quantification (niBAQ) values are shown for RPs of the small subunit (SSU, *Upper*) and the large subunit (LSU, *Lower*). Values are presented as mean ± SD ($n = 5$) (see Dataset S1 for values). (*B*) Agarose gel electrophoresis (*Left*) of nuclear RNA purified from cells pulse labeled with [^{3}H]-methyl-methionine. The gels show the [^{3}H]-methyl-methionine incorporation in the 45S/47S pre-RNA (*Upper*), and the corresponding band stained with ethidium bromide as a loading control (*Lower*). The radioactive signal was normalized against the ethidium bromide signal (*Right*). Values are presented as mean ± SD ($n = 2$). See also Fig. S1 and Dataset S1.

Altogether, these findings revealed that altering FBL expression in HeLa cells impacted ribosome biogenesis, notably rRNA maturation. However, although 2′-O-Me had decreased, the cytoplasmic ribosomes presented a normal protein composition.

***FBL* Knockdown Impacts 2′-O-Me of Nucleotides in a Site-Specific Manner, Including Nucleotides at Key Positions Within the Ribosome.** To identify potential site-specific methylation events and to quantify individual variations following *FBL* knockdown, we analyzed the methylation frequency of every nucleotide known to be ribose-methylated in human ribosomes (10). Several RNA-Seq–based 2′-O-Me mapping methods have been developed and used to refine the map of rRNA 2′-O-Me; however, these methods have so far not been applied to studying the dynamics of individual rRNA 2′-O-Me (9, 10, 28). We modified and applied our recently developed high-throughput RiboMethSeq technology (9) to human rRNA. RiboMethSeq is based on the protection of RNA hydrolysis provided by the methyl group, and on high-throughput sequencing to quantify the fraction of methylated nucleotides. The calculated MethScore represents the fraction of methylated rRNA at a given nucleotide in the ribosomal population (see *Materials and Methods* for details). We first established a reference map of rRNA 2′-O-Me in HeLa cells, using three independent biological replicates (Fig. 2). All of the 106 previously validated 2′-O-methylated nucleotides were highly methylated in rRNA of HeLa cells, except the 18S-Gm1447 nucleotide (MethScore = 0.09 ± 0.08). This was likely not due to a technical bias, since high MethScore values for this position were obtained in other cell lines. The majority of 2′-O-Me sites were methylated in over 80% of ribosomes, and only 16 sites (15%) were less-frequently methylated (MethScore ranging from 0.2 to 0.8). Among the sites conserved between yeast and human, all except one belonged to the highly methylated category (MethScore > 0.8), which is consistent with a high frequency of methylation of these nucleotides in yeast rRNA (9, 27). MethScore of individual sites displayed low dispersion among biological replicates, with a mean SD of 2.9%. Of the 106 known sites, 100 sites showed a level of variability below 5%, whereas only two sites in the 18S rRNA (Gm1447 and Cm174) and one in the 28S rRNA (Am4560) showed variability exceeding 10% (Fig. S2 and Dataset S2). This indicates that RiboMethSeq provides a robust measurement of 2′-O-Me levels. Altogether, these results demonstrate that the rRNA 2′-O-Me pattern is heterogeneous among human ribosomes.

RiboMethSeq was then applied to analyze the rRNA 2′-O-Me pattern upon *FBL* knockdown. Importantly, the transfection procedure did not introduce any experimental bias (Fig. S3*A*). Upon *FBL* knockdown, the frequency of 2′-O-Me decreased at almost all sites, although this variation was not statistically significant for all of the positions (Fig. 3*A*, Fig. S3 *B* and *C*, and Dataset S2). Surprisingly, the decrease in methylation was very different among sites, ranging from 0.2 to 57% (Fig. S3*C*), indicating that 2′-O-Me is likely controlled in a site-specific manner rather than systemically. The level of methylation significantly decreased for 59 sites ($P < 0.05$; 10 in 18S rRNA, 1 in 5.8S rRNA and 48 in 28S rRNA) (Dataset S2). Interestingly, each site with an initial methylation level below 80% decreased by at least an additional 10% upon *FBL* knockdown, suggesting that partial methylation might render these sites more sensitive to *FBL* knockdown, or that they are intrinsically prone to variation (Fig. S3*D*). Of note, the decrease in 2′-O-Me was greater for 28S rRNA than for 18S rRNA, which we attributed to the lower turnover of the 18S rRNA in *FBL* knockdown cells (Fig. S1*D*).

Because a majority of 2′-O-methylated nucleotides are localized within functional domains of the rRNA, as evidenced by 2D maps of rRNAs (11), we investigated whether the nucleotides displaying an altered 2′-O-Me upon *FBL* knockdown were localized in particular domains within the ribosome structure. Each 2′-O-Me site was mapped on the 3D structure of the HeLa cell 80S ribosome recently obtained by cryo-EM (29), and was assigned a color based on the decrease in methylation in *FBL* knockdown cells, according to four different groups (Fig. 3 *B* and *C* and Dataset S3). Affected sites (yellow, orange, and red in Fig. S3*E*) were distributed throughout the ribosome structure, including in the "core" of the ribosome, the most conserved region compared with bacterial ribosomes (30). Strikingly, several affected 2′-O-Me sites were located in regions that are known to be involved in the translational process, in particular close to the A and P-sites, the intersubunit bridges, and the peptide exit tunnel (Fig. 3*B* and Fig. S3*F*), demonstrating that these important regions are subjected to variations in methylation. In contrast, 2′-O-Me sites close to the peptidyl transferase center (PTC) were not affected, indicating that this functional region might be protected from variations in methylation (Fig. 3*C*). The decoding center within 18S rRNA was also devoid of altered sites (Fig. S3*G*).

In conclusion, these data demonstrate that the down-regulation of FBL, a factor of the general ribose methylation machinery, induces site-specific modulation of the 2′-O-Me pattern. While several functional domains of the ribosome are subjected to 2′-O-Me variation, other key domains might be protected.

2′-O-Me Inhibition Selectively Modifies the Intrinsic Capability of Ribosomes to Initiate Translation from Dicistrovirus IRES Elements and Not from the m^7G-Cap. To evaluate whether FBL knockdown impacts protein synthesis at a global level, we performed both a puromycylation assay (31), the signal produced by which represents the number of nascent peptides (Fig. S4 *A* and *B*), and an isotope pulse labeling with [^{35}S]-labeled amino acids, to evaluate the rate of amino acid incorporation (Fig. 4*A* and Fig. S4*C*). The results show a decrease in global synthesis of proteins, which indicates a reduction in the number of actively translating ribosomes, and is consistent with a decrease in ribosome production (Fig. S1*E*). Next, we sought whether *FBL* knockdown selectively altered mRNA translation. For this we applied ribosome profiling on HeLa cell lines expressing a FBL shRNA or a CTRL shRNA in an

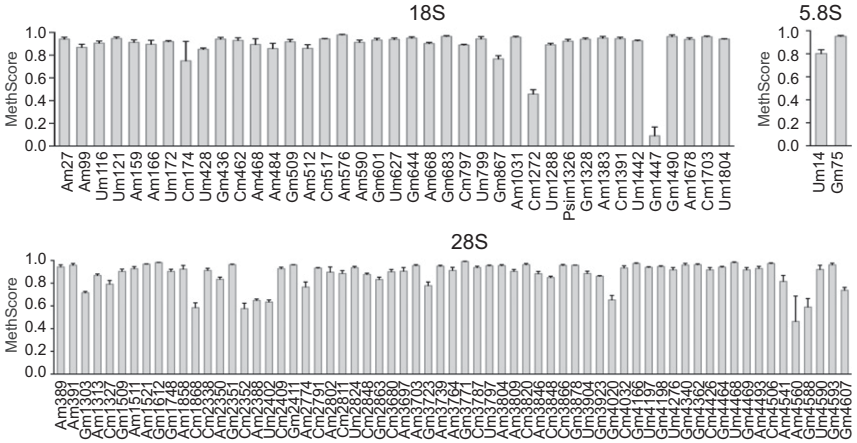

Fig. 2. Quantitative mapping of rRNA 2′-O-Me in human cells. The 2′-O-Me levels at each site of 18S, 28S, and 5.8S rRNA, evaluated by RiboMethSeq on nontreated HeLa cell rRNA. Data are expressed as mean MethScore values ± SD ($n = 3$ independent biological replicates) for each known methylated nucleotide in 18S, 5.8S, and 28S human rRNA. See also Fig. S2.

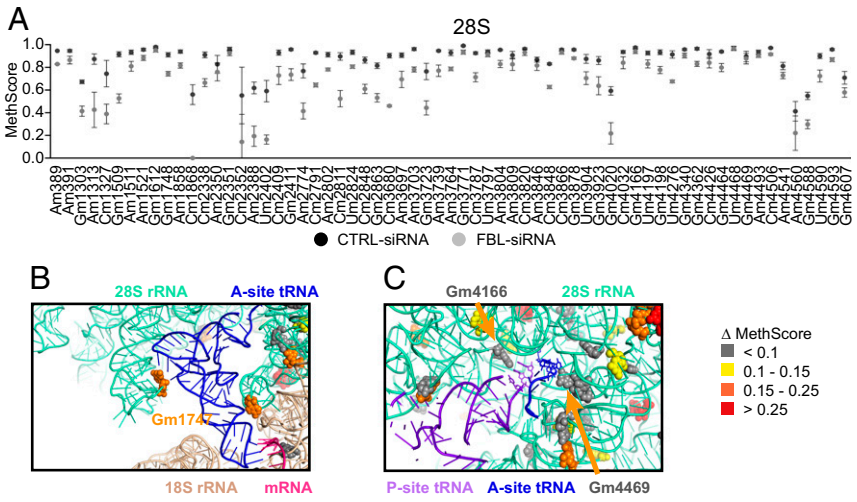

Fig. 3. *FBL* knockdown impacts 2′-O-Me of nucleotides in a site-specific manner, including nucleotides at key positions within the ribosome. (*A*) Mean MethScore values ± SD ($n = 3$ independent biological replicates) for each methylated nucleotide in 28S rRNA from HeLa cells transfected with CTRL-siRNA (black circle) or FBL-siRNA (gray circle). (*B*) View of the A-site in a HeLa cell ribosome 3D structure. Methylation sites are color coded according to the variation in MethScore comparing FBL siRNA cells with CTRL siRNA cells, as indicated on the right. The Gm1747 methylation site (orange, methylation decreased by 16.7%), is oriented with the 2′OH group close to the D-loop of the A-site tRNA (blue). (*C*) View of the PTC showing the tRNAs in the A-site (blue) and P-site (purple). Methylation frequency of nucleotides Gm4469 and Gm4166 (Gray) was not altered by *FBL* knockdown. See also Fig. S3 and Datasets S2 and S3.

inducible manner (Fig. S4 *D*, *F*, and *G*). Notably, change in the 2′-O-Me pattern, analyzed by RiboMethSeq, was similar after *FBL* knockdown induced by shRNA compared with the one induced by siRNA (Fig. S4*E*). Upon *FBL* knockdown, several genes were translationally altered (Fig. 4*B*). Translation efficiency of altered genes was either higher ($n = 28$) or lower ($n = 22$). This observation further supported that FBL, and possibly 2′-O-Me, could selectively regulate the translation efficiency of particular mRNA, although in this cellular model, there was no enrichment in particular molecular or cellular function (Fig. 4*B*).

Changes in *FBL* expression have been associated with alterations in IRES-dependent translation initiation (7, 22, 23). Within the subset of translationally altered mRNAs, 8% (four mRNAs) were previously identified in a large-scale screen for mRNAs able to drive Cap-independent translation (32). As a readout of changes in ribosome behavior, we analyzed IRES-dependent translational initiation in cellulo for a panel of cellular and viral IRESs using bicistronic constructs that code for two luciferases, the translation of which is either driven by the m^7G-cap (*Renilla* luciferase) or by an IRES structure (firefly luciferase) (Fig. S4*H*). The firefly/*Renilla* ratio revealed that *FBL* knockdown induced a decrease in translation initiation from cellular IRESs of FGF1, IGF-1R, and from the type II encephalomyocarditis virus (EMCV) IRES, but not from VEGFA IRES (Fig. 4*C*). Consistently, luciferase activity/mRNA ratios, which reflect translation efficiency, showed a decrease in Cap-dependent translation consistent with the global protein synthesis reduction observed in FBL-siRNA cells (Fig. 4*A*), and a stronger decrease in IRES-dependent translation (Fig. S4*I*). Thus, *FBL* knockdown alters IRES-dependent translational initiation with a selective impact depending on the nature of the IRES.

To determine whether altering the pattern of rRNA methylation directly contributes to the FBL-induced reduction in IRES-dependent translation, we analyzed the impact of *FBL* knockdown on translation initiation using the cricket paralysis virus intergenic region (CrPV-IGR) IRES, which is able to trigger the assembly of an active 80S ribosome in the absence of any cellular translation initiation factor (33). First, we observed that translation initiation from the CrPV-IGR IRES was significantly reduced upon *FBL* knockdown compared with control cells using a bicistronic construct (Fig. 4*D*). Second, to consolidate these data and further exclude the contribution of other factors involved in translation, such as tRNA, mRNA, or miRNA, we analyzed the translational capability of ribosomes extracted from *FBL* knocked-down cells in a hybrid in vitro translation assay, which we developed recently (34) (Fig. 4*E*). In this assay all of the translation machinery components, except for the ribosomes, are provided as purified products so that the cell-extracted ribosomes are the only variable components (see *Materials and Methods* for details). In this context, translation initiation from a Cap-less mRNA containing the CrPV-IGR IRES was severely impaired using ribosomes from *FBL* knockdown cells (Fig. 4*F*). In contrast, m^7G-cap–driven translation from mRNAs containing the GAPDH or globin 5′UTR, was not significantly affected (Fig. 4*F*). In addition to the CrPV-IGR IRES element, translation from the *Drosophila* C virus (DCV) IRES, another dicistrovirus type IV IRES, and from the type II IRES EMCV was also strongly impaired (Fig. S4*J*). Any artifact due to nonspecific binding of mRNA to ribosomes was excluded by reproducing the experiment using a range of mRNA:ribosome ratios (Fig. S4 *K* and *L*). In conclusion, these data demonstrate that modulation of the 2′-O-Me pattern alters the intrinsic capability of ribosomes to initiate translation from IRES elements, but not from the m^7G-cap structure of mRNAs.

Discussion

The most abundant modification in human rRNA, 2′-O-Me, is a highly complex and specific posttranscriptional modification, which is present in functionally important domains of the ribosome, indicating a significant contribution to ribosome functioning. However, existence of distinct 2′-O-Me patterns and the direct contribution of 2′-O-Me on the translational activity of ribosomes remain to be demonstrated. Here we show that rRNA 2′-O-Me patterns can be extensively modulated, although in a site-specific manner, including sites present in known functional regions of the ribosome, demonstrating that 2′-O-Me is a regulated, complex, and plastic feature of human ribosomes, and a molecular mechanism controlling ribosome functioning.

RiboMethSeq represents a unique method to simultaneously map and quantify 2′-O-Me on each site present in human rRNA, and was used here to explore the dynamics of 2′-O-Me. In HeLa cells, addition of 2′-O-Me appeared to be highly efficient since the majority of sites were methylated in almost 100% of the ribosomes. However, in contrast to yeast rRNA (9), a subset of sites was partially methylated, which has several conceptual implications: first, 2′-O-Me is not constitutively added at all sites in each ribosome; second, cells tolerate the production of ribosomes lacking some 2′-O-Me; and third, 2′-O-Me is a source of heterogeneity for the ribosomal population. In addition, a decrease in methylation was observed as a consequence of *FBL* knockdown (Fig. 3), and establishes 2′-O-Me as an adjustable and dynamic process, and a source of ribosome diversity. Subsequently, 2′-O-Me sites unaffected or weakly affected by *FBL* knockdown may represent sites for which methylation is highly efficient, or for which absence of methylation cannot be tolerated during ribosome biogenesis and subsequent quality control of ribosome fitness. The presence of 12 sites with a decrease in methylation exceeding 30% implies that *FBL* knocked-down cells contain ribosomes lacking 2′-O-Me at several sites. Consequently, 2′-O-Me should be considered and studied as a combination of sites, and

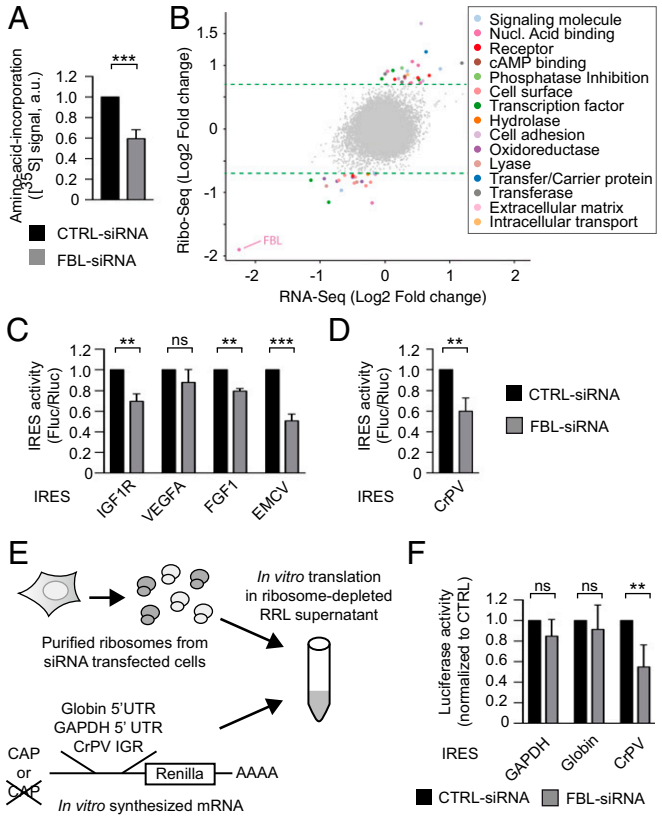

Fig. 4. 2′-O-Me inhibition selectively modifies the intrinsic capability of ribosomes to initiate translation from dicistrovirus IRES elements and not from the m^{7}G-cap. (*A*) Global protein synthesis was measured by incorporation of [^{35}S]-methionine–[^{35}S]cysteine labeling following SDS/PAGE and counting of radioactive signals. Values are presented as mean ± SD ($n = 4$). (*B*) Comparative mRNA translation by ribosome profiling on HeLa cells expressing either a CTRL-shRNA or a FBL-shRNA. Fold-changes at mRNA and translation levels are plotted along the *y* and the *x* axes, respectively. Translationally altered mRNA are colored according to their molecular function. Dotted green lines represent the significance threshold. (*C*) IRES-dependent translation (Fluc/Rluc) from several IRES elements was measured in HeLa cells transfected with CTRL-siRNA (black bars) or FBL-siRNA (gray bars). Values are presented as mean ± SD ($n = 3$). (*D*) Identical experimental set-up as in *D* using a reporter construct carrying the CrPV-IGR IRES element. Values are presented as mean ± SD ($n = 3$). (*E*) Schematic representation of the hybrid in vitro translation assay. (*F*) In vitro translation was evaluated by measuring luciferase activity produced with 1 μg of ribosomes. Cap-dependent translation was evaluated using reporter constructs containing the 5′UTR of GAPDH or globin mRNA. IRES-dependent translation was evaluated using a Cap-less mRNA containing the CrPV-IGR IRES as 5′UTR. ns, not significant; $^{**}P \leq 0.01$; $^{***}P \leq 0.001$. See also Fig. S4.

not only individually, consistent with data obtained using snoRNA knockout yeast strains (12, 13).

FBL knockdown induced an unexpected site-specific alteration of 2′-O-Me (Fig. 3) by mechanisms that need to be further studied. Changes in single 2′-O-Me sites were not correlated with the global level of the corresponding snoRNA guide, further supporting that snoRNA expression by itself is not the main mechanism regulating 2′-O-Me (10). Possibly, the efficiency of methylation might be disproportionate among snoRNPs. The site-specific impact of *FBL* knockdown shows that modulating the expression of common components of the methylation machinery represents a means of regulating 2′-O-Me patterns. It follows that the steep down-regulation of FBL observed during neurogenesis and stem cell differentiation (20, 21) may affect rRNA 2′-O-Me patterns, with a direct impact on ribosome function. Conversely, overexpression of *FBL* in tumors and cancer cells might increase 2′-O-Me at selected sites, as suggested by our previous data (7). The moderate impact on ribosome production (Fig. S1*E*) and absence of detectable consequences on ribosomal protein assembly and stoichiometry provides additional quantitative biochemical evidence that FBL regulates protein synthesis through its impact on 2′-O-Me plasticity (7). Therefore, *FBL* regulation may represent a means of modulating the 2′-O-Me pattern of rRNA without adversely impacting overall ribosome production.

In this study, we used translation initiation from Cap and IRES structures as functional assays to assess changes in behavior of ribosomes. The decrease in CrPV IRES activity in in cellulo and in vitro assays demonstrates that ribosomes with an altered 2′-O-Me pattern become intrinsically less efficient at initiating translation from IRES elements, in a manner independent of translation initiation factors. The decrease in EMCV IRES activity in our in vitro assay (Fig. S4*J*) reveals that 2′-O-Me impacts different types of IRESs, and further supports that 2′-O-Me is responsible for the FBL-dependent regulation of IRES-containing cellular mRNAs (7) (Fig. 4*C*). IRES elements recruit the 40S subunit through different interacting pathways involving eIF, but also ribosomal proteins, such as RPS25 (35). This raises the possibility that 2′-O-Me controls IRES translation via RPs, although our proteomic analysis demonstrates that 2′-O-Me alterations did not induce significant changes in RP composition, thus excluding that the decrease in IRES translation originated from a loss of RP, such as RPS25. Cap-independent translation of cellular mRNAs appears more widespread than anticipated, and comprises mechanisms based on direct interaction between mRNAs and 18S rRNA, in a Shine d'Algarno-like manner (32). Such a mechanism might thus be more sensitive to chemical modifications of rRNA. Importantly, rRNA 2′-O-Me provides selectivity to the translation machinery toward a subset of mRNAs (Fig. 4 *B* and *C*). Additional studies are necessary to characterize mRNAs, the translation of which is regulated through rRNA 2′-O-Me.

The limited impact observed on translation from globin and GAPDH 5′UTR in the in vitro translation assay indicates that 2′-O-Me does not significantly modulate the ability of ribosomes to initiate Cap-dependent translation. This suggests that the decrease in global protein synthesis observed in cellular assays (Fig. 4*A* and Fig. S4*C*) is related to the lower ribosome production in *FBL* knockdown cells. Nevertheless, at this point we cannot exclude that 2′-O-Me affects some of the Cap-dependent pathways, and additional studies will be necessary to evaluate the impact of 2′-O-Me on the different mechanisms of Cap-dependent translation initiation. In addition, the limited impact of 2′-O-Me on Cap-dependent translation in the in vitro translation assay, also indicates that there was no major defect in translation elongation. Data from [^{35}S]-methionine–[^{35}S]cysteine pulse labeling, which reflect the rate of amino acid incorporation, and data from puromycylation assays, which reveal the number of ribosomes engaged in translation, both showed similar alterations upon FBL knockdown, and further indicate that elongation rate is similar in FBL knockdown cells compared with control cells. The impact of 2′-O-Me on synthesis of proteins, which are sensitive to translation elongation rate, remains to be studied. These observations unambiguously demonstrate that 2′-O-Me contributes to the translational activity of the ribosome.

The role of 2′-O-Me on ribosome structure and function is not known. Mapping of 2′-O-Me sites onto the ribosome structure revealed that 2′-O-Me can be modulated in several regions involved in intermolecular interactions, such as between tRNA and the A-site (Fig. 3*B*), intersubunit bridges (Fig. S3*F*), or around the peptide exit tunnel. The importance of 2′-O-Me at these locations was demonstrated in yeast and should now be explored in human models (11). Equally important are functional regions that did not display variations in 2′-O-Me. In particular, the 2′-O-Me sites of the PTC were unaltered, strongly indicating that this region is protected from 2′-O-Me variation. Therefore, our study supports the notion that 2′-O-Me comprises constitutively modified sites and regulated sites. How 2′-O-Me contributes to the molecular structure of the ribosome remains to be determined. Recent high-resolution crystal structures of the *Thermus thermophilus* ribosome and cryo-EM structures of human ribosomes, showed that the ribose 2′-O positions of several nucleotides are directly involved in

molecular interactions, both in a methylated and unmethylated state (29, 36). It can be anticipated that these interactions would be disrupted upon changes in methylation of these nucleotides, and may impact elongation and termination, in addition to initiation. However, technological advances in structural tools available today, such as cryo-EM and X-crystallography, are required to obtain a finer view of the structure–function relationship of human 2′-O-Me patterns.

In conclusion, 2′-O-Me plasticity reported herein expands the repertoire of ribosome composition and further demonstrates the existence of diversity in ribosome populations. The impact on the intrinsic ribosomal functioning establishes 2′-O-Me plasticity as a molecular mechanism modulating ribosomal activity, and further supports that modifications in rRNA chemical patterns, including pseudouridylation and base modifications, mediate ribosome functional specialization. These data expose the ribosomal RNA epitranscriptome as a new level of regulation of gene expression.

Materials and Methods

Detailed experimental procedures are described in *SI Materials and Methods*.

Ribosome Protein Composition. Ribosomes composition was analyzed by label-free quantitative proteomics as described previously (37, 38).

Analysis of rRNA Methylation. Site-specific rRNA methylation was determined by RiboMethSeq, as previously described (9).

Ribosome Structure Analysis. Methylated nucleotides were mapped on the cryo-EM structure of the human ribosome (PDB ID code 4UG0) (29). The reference structure of prokaryotic ribosome containing A-, P-, and E-site tRNAs plus mRNA was from *T. thermophilus* (PDB ID code 4V5C) (39).

Translation Assay. Global protein synthesis was performed as previously described (40). In cellulo translation assays using bicistronic vectors and in vitro translation were performed as described previously (7, 34, 41).

Ribosome Profiling. Ribosome profiling was performed as previously described (42). Gene Ontology (GO) terms were identified for genes showing a significant expression variation using Panther (43).

ACKNOWLEDGMENTS. We thank A.-C. Prats and D. Ruggero for kindly providing internal ribosome entry site-containing vectors; D. Lafontaine for discussion; and Brigitte Manship for editing the manuscript. Microscopic imaging was performed using the Centre de Recherche en Cancérologie de Lyon imaging platform. The project was funded by Agence Nationale pour la Recherche (RIBOMETH ANR-13-BSV8-0012-01); the "Programmes d'Actions Intégrées de Recherche" RiboTEM (PAIR, Institut National du Cancer, Fondation ARC pour la Recherche sur le Cancer, Ligue Nationale Contre le Cancer); the "Ligue Nationale Contre le Cancer"; the "Ligue Contre le Cancer, Comité Départemental de la Drôme, du Rhône, du Puy-de-Dôme, et de l'Allier"; and Fondation ARC pour la Recherche sur le Cancer. F.C. is a CNRS research fellow. J.-J.D., and V. Marcel are INSERM research fellows. M.G. was supported by Agence Nationale pour la Recherche Grant "INVADE" PC201507. F.L. received a PhD fellowship from the French Ministry for Research and Education. V. Marchand and Y.M. were supported by joint Agence Nationale de la Recherche -Deutsche Forschungsgemeinschaft Grant HTRNAMod (ANR-13-ISV8-0001/HE 3397/8-1). Y.C. and A.A. were supported by the bottom-up platform and informatics group at Exploring the Dynamics of Proteomes (EDyP). Proteomic experiments were partly supported by the ProFi Grant ANR-10-INBS-08-01. M.M. and M.Y. were supported by European Research Council advanced Grant 294312. M.Y. was supported by the Russian Government Program of Competitive Growth of Kazan Federal University. This work has benefited from the platform and expertise of the High-throughput Sequencing Platform of Institute for Integrative Biology of the Cell (I2BC).

1. Schwanhäusser B, et al. (2011) Global quantification of mammalian gene expression control. *Nature* 473:337–342.
2. Hinnebusch AG, Ivanov IP, Sonenberg N (2016) Translational control by 5′-untranslated regions of eukaryotic mRNAs. *Science* 352:1413–1416.
3. Hoernes TP, Erlacher MD (2017) Translating the epitranscriptome. *Wiley Interdiscip Rev RNA* 8:e1375.
4. Xue S, Barna M (2012) Specialized ribosomes: A new frontier in gene regulation and organismal biology. *Nat Rev Mol Cell Biol* 13:355–369.
5. Xue S, et al. (2015) RNA regulons in Hox 5′ UTRs confer ribosome specificity to gene regulation. *Nature* 517:33–38.
6. Majzoub K, et al. (2014) RACK1 controls IRES-mediated translation of viruses. *Cell* 159: 1086–1095.
7. Marcel V, et al. (2013) p53 acts as a safeguard of translational control by regulating fibrillarin and rRNA methylation in cancer. *Cancer Cell* 24:318–330.
8. Sharma S, Lafontaine DL (2015) 'View from a bridge': A new perspective on eukaryotic rRNA base modification. *Trends Biochem Sci* 40:560–575.
9. Marchand V, Blanloeil-Oillo F, Helm M, Motorin Y (2016) Illumina-based RiboMethSeq approach for mapping of 2′-O-Me residues in RNA. *Nucleic Acids Res* 44:e135.
10. Krogh N, et al. (2016) Profiling of 2′-O-Me in human rRNA reveals a subset of fractionally modified positions and provides evidence for ribosome heterogeneity. *Nucleic Acids Res* 44:7884–7895.
11. Decatur WA, Fournier MJ (2002) rRNA modifications and ribosome function. *Trends Biochem Sci* 27:344–351.
12. Liang XH, Liu Q, Fournier MJ (2007) rRNA modifications in an intersubunit bridge of the ribosome strongly affect both ribosome biogenesis and activity. *Mol Cell* 28:965–977.
13. Baudin-Baillieu A, et al. (2009) Nucleotide modifications in three functionally important regions of the Saccharomyces cerevisiae ribosome affect translation accuracy. *Nucleic Acids Res* 37:7665–7677.
14. Higa-Nakamine S, et al. (2012) Loss of ribosomal RNA modification causes developmental defects in zebrafish. *Nucleic Acids Res* 40:391–398.
15. Bortolin-Cavaillé ML, Cavaillé J (2012) The SNORD115 (H/MBII-52) and SNORD116 (H/MBII-85) gene clusters at the imprinted Prader-Willi locus generate canonical box C/D snoRNAs. *Nucleic Acids Res* 40:6800–6807.
16. Tollervey D, Lehtonen H, Jansen R, Kern H, Hurt EC (1993) Temperature-sensitive mutations demonstrate roles for yeast fibrillarin in pre-rRNA processing, pre-rRNA methylation, and ribosome assembly. *Cell* 72:443–457.
17. Rodriguez-Corona U, Sobol M, Rodriguez-Zapata LC, Hozak P, Castano E (2015) Fibrillarin from Archaea to human. *Biol Cell* 107:159–174.
18. Watkins NJ, Bohnsack MT (2012) The box C/D and H/ACA snoRNPs: Key players in the modification, processing and the dynamic folding of ribosomal RNA. *Wiley Interdiscip Rev RNA* 3:397–414.
19. Tessarz P, et al. (2014) Glutamine methylation in histone H2A is an RNA-polymerase-I-dedicated modification. *Nature* 505:564–568.
20. Recher G, et al. (2013) Zebrafish midbrain slow-amplifying progenitors exhibit high levels of transcripts for nucleotide and ribosome biogenesis. *Development* 140:4860–4869.
21. Watanabe-Susaki K, et al. (2014) Biosynthesis of ribosomal RNA in nucleoli regulates pluripotency and differentiation ability of pluripotent stem cells. *Stem Cells* 32:3099–3111.
22. Su H, et al. (2014) Elevated snoRNA biogenesis is essential in breast cancer. *Oncogene* 33:1348–1358.
23. Basu A, et al. (2011) Requirement of rRNA methylation for 80S ribosome assembly on a cohort of cellular internal ribosome entry sites. *Mol Cell Biol* 31:4482–4499.
24. Belin S, et al. (2009) Dysregulation of ribosome biogenesis and translational capacity is associated with tumor progression of human breast cancer cells. *PLoS One* 4:e7147.
25. Sornjai W, et al. (2017) Hypermethylation of 28S ribosomal RNA in beta-thalassemia trait carriers. *Int J Biol Macromol* 94:728–734.
26. Kos M, Tollervey D (2010) Yeast pre-rRNA processing and modification occur cotranscriptionally. *Mol Cell* 37:809–820.
27. Birkedal U, et al. (2015) Profiling of ribose methylations in RNA by high-throughput sequencing. *Angew Chem Int Ed Engl* 54:451–455.
28. Incarnato D, et al. (2016) High-throughput single-base resolution mapping of RNA 2′-O-methylated residues. *Nucleic Acids Res* 45:1433–1441.
29. Khatter H, Myasnikov AG, Natchiar SK, Klaholz BP (2015) Structure of the human 80S ribosome. *Nature* 520:640–645.
30. Ben-Shem A, et al. (2011) The structure of the eukaryotic ribosome at 3.0 Å resolution. *Science* 334:1524–1529.
31. David A, et al. (2012) Nuclear translation visualized by ribosome-bound nascent chain puromycylation. *J Cell Biol* 197:45–57.
32. Weingarten-Gabbay S, et al. (2016) Comparative genetics. Systematic discovery of cap-independent translation sequences in human and viral genomes. *Science* 351:aad4939.
33. Fernández IS, Bai XC, Murshudov G, Scheres SH, Ramakrishnan V (2014) Initiation of translation by cricket paralysis virus IRES requires its translocation in the ribosome. *Cell* 157:823–831.
34. Panthu B, Décimo D, Balvay L, Ohlmann T (2015) In vitro translation in a hybrid cell free lysate with exogenous cellular ribosomes. *Biochem J* 467:387–398.
35. Hertz MI, Landry DM, Willis AE, Luo G, Thompson SR (2013) Ribosomal protein S25 dependency reveals a common mechanism for diverse internal ribosome entry sites and ribosome shunting. *Mol Cell Biol* 33:1016–1026.
36. Polikanov YS, Melnikov SV, Söll D, Steitz TA (2015) Structural insights into the role of rRNA modifications in protein synthesis and ribosome assembly. *Nat Struct Mol Biol* 22:342–344.
37. Penzo M, et al. (2015) Human ribosomes from cells with reduced dyskerin levels are intrinsically altered in translation. *FASEB J* 29:3472–3482.
38. Casabona MG, Vandenbrouck Y, Attree I, Couté Y (2013) Proteomic characterization of *Pseudomonas aeruginosa* PAO1 inner membrane. *Proteomics* 13:2419–2423.
39. Voorhees RM, Weixlbaumer A, Loakes D, Kelley AC, Ramakrishnan V (2009) Insights into substrate stabilization from snapshots of the peptidyl transferase center of the intact 70S ribosome. *Nat Struct Mol Biol* 16:528–533.
40. Bash-Imam Z, et al. (2017) Translational reprogramming of colorectal cancer cells induced by 5-fluorouracil through a miRNA-dependent mechanism. *Oncotarget* 8:46219–46233.
41. Jack K, et al. (2011) rRNA pseudouridylation defects affect ribosomal ligand binding and translational fidelity from yeast to human cells. *Mol Cell* 44:660–666.
42. Baudin-Baillieu A, et al. (2014) Genome-wide translational changes induced by the prion [PSI+]. *Cell Rep* 8:439–448.
43. Mi H, et al. (2017) PANTHER version 11: Expanded annotation data from gene ontology and reactome pathways, and data analysis tool enhancements. *Nucleic Acids Res* 45:D183–D189.

Supporting Information

Erales et al. 10.1073/pnas.1707674114

SI Materials and Methods

Cell Culture and siRNA Transfection. HeLa cells (ATCC) were grown in Minimum Essential Medium supplemented with 10% FBS, glutamine, and nonessential amino acids at 37 °C with 5% CO_2. For siRNA experiments, three siRNA duplexes were used for fibrillarin silencing: 5′-GUCUUCAUUUGUCGAGGAA-AdTdT-3′; 5′-UGGAGGACACUUUGUGAUUUUdtdT-3′; and 5′-CUGUCAGGAUUGCGAGAGAdTdT-3′.

The control siRNA does not target any human sequence (negative control siRNA duplex; Eurogentec). HeLa cells were transfected using the X-tremeGENE siRNA reagent (Roche) according to the manufacturer's instructions. Seventy-two hours after siRNA transfection, cells were plated according to future analyses.

Transfection and Plasmid Construction. For siRNA experiments, plasmids containing the bicistronic IRES luciferase constructs were described previously (7, 41).

Dual Luciferase Assays for in Cellulo Translation Assays. pIRES-FGF1, pIRES-EMCV, and pIRES-VEGFA were donated by A. C. Prats, Institut des Maladies Métaboliques et Cardiovasculaires, Toulouse, France and pRF-CrPV was a gift from D. Ruggero, University of California, San Francisco. Luciferase assays were performed 24 h after transfection with the reporter plasmids using X-tremeGENE 9 reagent (Roche). Dual luciferase assays were performed using the Dual-Glo luciferase reagent (Promega) according to the manufacturer's instructions, and a Tecan M1000 plate reader. IRES translation initiation is the ratio of background subtracted signal of Firefly luciferase over *Renilla* luciferase.

Global Protein Synthesis. Global protein synthesis analysis by puromycylation followed by puromycin detection was performed essentially as in ref. 31. Puromycin incorporation was detected by Western blot on whole-cell protein extracts. Global protein synthesis by isotope labeling was performed as previously described (46) by incubating cells for 30 min, with a [^{35}S]-methionine–[^{35}S]cysteine mix. Proteins were separated by SDS/PAGE on a 4–15% gradient polyacrylamide gel (Bio-Rad).

Real-time quantitative RT-PCR. Two-hundred nanograms of total RNA were reverse transcribed using the MMLV RT kit and random primers (Invitrogen), according to the manufacturer's instructions. Quantitative real-time PCR (RT-qPCR) was carried out using the Light cycler 480 II real-time PCR thermocycler (Roche). Expression of mRNAs was quantified using LightCycler 480 SYBR Green I Master Mix (Roche) and normalized using HPRT1 expression according to the 2-ΔΔCt method.

Primers were as follows: LucR-Fwd 5′-AACGCGGCCTCT-TCTTATTT, LucR-Rev 5′-ACCAGATTTGCCTGATTTGC, LucF-Fwd 5′-AACACCCCAACATCTTCGAC, LucF-Rev 5′-TTTTCCGTCATCGTCTTTCC, HPRT1-Fwd 5′-TGACACTG-GCAAAACAATGCA, HPRT1-Rev 5′-GGTCCTTTTCACCAG-CAAGCT.

Immunofluorescence analysis. Cells were grown on glass coverslips, fixed in 4% of paraformaldehyde in PBS before permeabilization with 0.5% Triton X-100 in PBS. Fibrillarin and nucleolin were detected using the anti-FBL rabbit polyclonal antibody (ab5821; Abcam) diluted at 1:2,000, and the anti-NCL mouse monoclonal antibody (ab13541; Abcam) at 1:4,000. Secondary antibodies were labeled with AlexaFluor488 or AlexaFluor555 (Molecular Probes), and used at 1:1,000. Coverslips were mounted using the Fluoromount G mounting medium (EMS). Images were acquired on a Nikon NiE fluorescence microscope using a 60× Plan Apochromat immersion objective (NA 1.4) and a Flash 4.0 CMOS camera (Hammamatsu).

Ribosome purification. Ribosomes were purified as previously described (24). Briefly, cytoplasmic fractions were obtained by mechanical lysis of cells with a Dounce and centrifugation at 12,000 × *g* for 10 min to pellet mitochondria. Cytoplasmic fractions were loaded onto a 1 M sucrose cushion in a buffer containing 50 mM Tris·HCl pH 7.4, 5 mM $MgCl_2$, 500 mM KCl, and 2 mM DTT, and centrifuged for 2 h at 240,000 × *g*. The pellet containing the ribosomes was suspended in a buffer containing 50 mM Tris·HCl pH 7.4, 5 mM $MgCl_2$, and 25 mM KCl.

Ribosome Production. Ribosome production was measured as described previously (24). Briefly, cells were incubated for 1 h in methionine-cysteine-free DMEM supplemented with a [^{35}S]-methionine–[^{35}S]cysteine mix (GE Healthcare). Incorporation of radioactive amino acids was measured from one unit ($OD_{260\ nm}$).

Two-dimensional gel electrophoresis. For 2D gel electrophoresis, 5 $OD_{260\ nm}$ units of ribosomes extracted from [^{35}S]-methionine–[^{35}S]cysteine-labeled cells were used. The method was previously described (24). Briefly, ribosomal proteins were extracted using acetic acid, extensively dialyzed against 1 M acetic acid and lyophilized. After lyophilizing, proteins were solubilized and reduced in 6 M guanidine hydrochloride, 0.5 M Tris·HCl pH 8.5 and 10 mM DTE. Proteins were then alkylated by adding 40 mM iodoacetamide in 6 M guanidine hydrochloride and 0.5 M Tris-HCl pH 8.5. Proteins were lyophilized and solubilized in sample buffer (20 mM Tris-boric acid pH 8.3, 1 mM EDTA and 8 M urea).

In the first dimension, proteins were separated according to their electric charge, in 4% polyacrylamide gels containing 0.2 M Tris-boric acid pH 8.6, 8 M urea, and 10 mM EDTA, placed in glass tubes. At the end of the first dimensional run, gels were extracted from the tube and equilibrated for 5 min in 0.625 M Tris·HCl pH 6.8, 2% SDS, and 0.002% Bromophenol blue. For the second dimension, the gels from the first dimension were placed in a 1.5-mm-thick gel cast made of 14% polyacrylamide (37.5:1 acrylamide: *N*-*N*′methylenebisacrylamide). Protein separation was achieved using standard SDS/PAGE conditions. Proteins were stained by 0.1% Coomassie brilliant blue R 250. Gels were dried and exposed to PhosphoImaging screen. All chemicals were purchased from Sigma-Aldrich.

Mass spectrometry-based proteomic analyses of purified ribosomes. Label-free quantitative proteomics has been performed as in Casabona et al. (38). Ribosomes purified at 500 mM KCl were solubilized in Laemmli buffer, stacked in the top of a 4–12% NuPAGE gel (Invitrogen), and stained by R-250 Coomassie blue (Bio-Rad). Gel bands were excised and in-gel proteins were digested using trypsin (Promega). Resulting peptides were analyzed by nanoliquid chromatography coupled to tandem mass spectrometry (Ultimate 3000 coupled to LTQ-Orbitrap Velos Pro; Thermo Scientific) using a 120-min gradient. RAW files were processed using MaxQuant v1.5.3.30. Spectra were searched against the SwissProt database (*Homo sapiens* taxonomy, October 2016 version) and the frequently observed contaminants database embedded in MaxQuant. Trypsin was chosen as the enzyme and two missed cleavages were allowed. Precursor mass error tolerances were set respectively at 20 ppm and 4.5 ppm for first and main searches. Fragment mass error tolerance was set to 0.5 Da. Peptide modifications allowed during

the search were: carbamidomethylation (C, fixed), acetyl (Protein N-ter, variable) and oxidation (M, variable). Minimum peptide length was set at seven amino acids. Minimum number of peptides, razor + unique peptides and unique peptides were all set at 1. Maximum false-discovery rates (FDR)—calculated by employing a reverse database strategy—were set at 0.01 at peptide and protein levels. iBAQ values were calculated from MS intensities of unique + razor peptides and used for statistical analyses using ProStar. Proteins identified in the reverse and contaminant databases or exhibiting less than 5 iBAQ values in one condition were discarded from the matrix. After $\log_2$ transformation, iBAQ values were median-normalized, missing data imputation was carried out (replacing missing values by the 2.5-percentile value of each column) and statistical testing was conducted using the *limma t* test. Differentially expressed proteins were sorted out using a $\log_2$ (fold-change) cut-off of 2, and a FDR threshold on *P* values of 1% using the Benjamini–Hochberg method.

For generation of Fig. 1*C*, iBAQ values from ribosomal proteins were sorted out before column-wise normalization; to facilitate representation (data centering on 1), for each ribosomal protein the normalized iBAQ values were divided by the mean of the 10 values obtained.

Western blot analysis. Twenty micrograms of total protein lysates were run on a 12% SDS polyacrylamide gel and transferred onto a nitrocellulose membrane. The membrane was blocked with 3% nonfat milk in TBST. The antibodies used were the following: fibrillarin (ab166630; Abcam) at 1:2,000, Dyskerin (sc-48794; Santa Cruz) at 1:500, nucleophosmin (sc-5564; Santa Cruz) at 1:500, puromycin (clone 12D10; EMD Millipore) at 1:4,000, and Ku80 (ab3715; Abcam) at 1:2,000. Antibodies were incubated for 1 h in 1% milk-TBST. Proteins were detected by chemiluminescence using an anti-rabbit or anti-mouse peroxidase-conjugated antibody (Cell Signaling) diluted 1:10,000, and Clarity ECL substrate (Bio-Rad). Images were collected on a ChemiDoc XRS+ (Bio-Rad) and the signal analyzed using the Bio-Rad ImageLab software.

Northern blot analysis. Northern blot was performed as described in Belin et al. (24). The probes were obtained by oligonucleotide synthesis (Eurogenetec): ETS1-1399–5′-CGCTAGAGAAGGCTTTTCTC-3′; ITS1-5′-CCTCTTCGGGGGACGCGCGCGTGGCCCCGA-3′; and ITS2-5′-GCGCGACGGCGGACGACACCGCGGCGTC-3′.

Next, 50 pmoles of each oligonucleotide probe was labeled in the presence of 50 pmoles of [γ-^{32}P] ATP (Perkin-Elmer) and T4 polynucleotide kinase (New England Biolabs) for 30 min at 37 °C.

Three micrograms of nuclear RNAs were resolved on a 1% denaturing agarose gel and blotted onto a Hybond-N+ membrane (GE Healthcare). Signal detection was performed using a PhosphorImager (FLA 9500; GE Healthcare). Total 28S and 18S rRNA were visualized by fluorescence imaging following ethidium bromide staining, and were used as loading controls.

Analysis of rRNA methylation by isotope labeling. Cells were incubated for 1 h in DMEM supplemented with 10% heat-inactivated dialyzed FCS and [^{3}H]-methyl-methionine at a final concentration of 15 μCi/mL (GE Healthcare). After 1-h labeling, cells were washed three times with ice-cold PBS, and scrapped. Nuclei were isolated by mechanical fractionation and nuclear RNAs were extracted and separated on formaldehyde agarose gels. RNAs were transferred onto nitrocellulose membranes. Radioactivity of the 45S/47S pre-rRNA was measured after exposure on a PhosphorImager screen, using a Typhoon scanner (GE Healthcare).

Analysis of rRNA methylation by RiboMethSeq. RiboMethSeq is based on protection of phosphodiester bonds against alkaline hydrolysis conferred by replacement of the 2′OH by a methyl group. The 3′-downstream nucleotide is thus absent at the 5′-end in the collection of RNA fragments. Partial alkaline hydrolysis of total RNA samples is followed by deep-sequencing and allows 5′-end counting for every fragment. The calculated MethScore represents the level of methylation of a given nucleotide in the ribosomal population.

RiboMethSeq was performed essentially as described previously (9), and is presented in detail below.

RNA fragmentation. RNA (1–250 ng) was subjected to alkaline hydrolysis in 50 mM bicarbonate buffer pH 9.2 for 4–10 min at 95 °C. The reaction was stopped by ethanol precipitation using 0.3 M Na-OAc pH 5.2 and glycoblue as a carrier in liquid nitrogen. After centrifugation, the pellet was washed with 80% ethanol and resuspended in nuclease-free water. The size of RNA fragments (30–200 nt) generated was assessed by capillary electrophoresis using a PicoRNA chip on Bioanalyzer 2100 (Agilent).

End repair of RNA fragments. Fragmented RNA without an additional fractionation step was 3′-end dephosphorylated using 5 U of Antartic Phosphatase (New England Biolabs) for 30 min at 37 °C and after inactivation of the phosphatase for 5 min at 70 °C, RNA was phosphorylated at the 5′-end using T4 PNK and 1 mM ATP for 1 h at 37 °C. End-repaired RNA was then purified using RNeasy MinElute Clean-up kit (Qiagen) according to the manufacturer's recommendations, except that 675 μL of 96% ethanol were used for RNA binding. Elution was performed in 10 μL of nuclease-free H_2O.

Library preparation. RNA was converted to a library using NEBNext Small RNA Library kit (New England Biolabs) following the manufacturer's instructions. Library quality was assessed using a High Sensivity DNA chip on a Bioanalyzer 2100. Library quantification was done using a fluorometer (Qubit 2.0 fluorometer; Invitrogen).

Sequencing. Libraries were multiplexed and subjected to high-throughput sequencing using an Illumina HiSEq. 1000 instrument with 50-bp single-end read runs. Since clustering of the short fragments was very efficient, libraries were loaded at a concentration of 6–8 pM per lane.

Bioinformatics pipeline. Adapter sequence trimming was done using Trimmomatic-0.32 with the following parameters: LEADING:30 TRAILING:30 SLIDINGWINDOW:4:15 MINLEN:17 AVGQUAL:30. Alignment to the reference rRNA sequence was done by Bowtie2 (v2.2.4) in End-to-End mode. The 5′-end counting was done directly on *.sam file using dedicated Unix script. Final analysis was performed by calculation of MethScore for quantification of 2′-O-Me residues.

Ribosome Structure Analysis. Methylated nucleotides were mapped on the cryo-EM structure of the human ribosome (PDB ID code 4UG0) (30). Reference structure of prokaryotic ribosome containing A-, P-, and E-site tRNAs plus mRNA was from *Thermus thermophilus* (PDB ID code 4V5C) (39). Observations of methylation site positions with regards to active sites of the ribosome were made after sequence alignment and structural superposition of the 23S rRNA of the *T. thermophilus* ribosome onto the 28S rRNA of human ribosome for the PTC and the CCA-end binding pocket of the E-site or sequence alignment and structural superposition of the 16S rRNA of the *T. thermophilus* ribosome onto the 18S rRNA of human ribosome for the decoding center and mRNA path. Figures and sequence alignment followed by structure superposition were performed using PyMOL 1.4 (Schrödinger; https://pymol.org/2/).

shRNA-Expressing Cells Lines. HeLa cell lines expressing an inducible shRNA were generated by lentiviral infection. Lentiviral particles were produced using the pTRIPZ-shRNA-NS and pTRIPZ-shRNA-FBL-351067 vectors, which were acquired from Open Biosystems (Dharmacon). Upon lentiviral infection, cell populations were selected using puromycin at 2 μg/mL for 14 d. Cells were grown under selection at 1 μg/mL and cultured without puromycin 24 h before any experiment. shRNA expression was induced by doxycycline treatment for 5 d at 1 μg/mL. Induction efficiency was monitored by evaluating the tRFP expression

marker, by observation under fluorescent microscope or by flow cytometry. Change in FBL levels was verified by Western blotting.

Ribosome profiling.

Ribosome protected fragments preparation and sequencing. HeLa ± FBL-shRNA cells were cultivated during 5 d with 1 μg/mL doxycycline. Next, 150 million cells were treated with 100 μg/mL cycloheximide for 10 min at 37 °C. Then, cells were suspended in lysis buffer (10 mM Tris-PO_4 pH7.5, 100 mM KCl, 10 mM Mg^{2+} acetate, 1% Triton X-100, 2 mM DTT, 100 μg/mL cycloheximide). Glass beads were added and cells were lysed by vortexing 5 min at 4 °C. The supernatant was collected and digested with 15 U RNase I AMBION/OD_{260} for 1 h at 25 °C. To purify monosomes, digested extracts were loaded on a 24% sucrose cushion (50 mM Tris-acetate pH 7.6, 50 mM NH_4Cl, 12 mM $MgCl_2$, 1 mM DTT) and centrifuged at 413,000 × *g* for 2 h 15 min. Pellets were washed with lysis buffer and suspended in the same buffer. Ribosome protected fragments (RPF) were purified by phenol-chloroform extraction, and suspended in Superase-IN AMBION solution (1 U/μL).

RPFs were purified on 16% (vol/vol) acrylamide-bisacrylamide (19:1) gel made with 7 M urea and 1× Tris-acetate-EDTA (TAE) buffer. After staining for 30 min in 1× SYBR Gold (Life Technologies) diluted in 1× TAE, RNA contained in the 28- and 34-nt regions were separately excised from the gel. The gels slices were stored at least 2 h at −20 °C and then physically disrupted. RNAs were eluted overnight from gel fragments by passive diffusion in 500 μL of RNA extraction buffer II (300 mM NaOAc pH 5.5, 1 mM EDTA) at 4 °C on a rotating wheel. After filtration, RPFs were precipitated in ethanol with 20 mg glycogen, suspended in 20 μL Superase-IN AMBION solution (1 U/μL), and stored at −80 °C until use.

Ribosome footprints were depleted from ribosomal RNA with the Ribo-Zero Human kit (Illumina) following the manufacturer's recommendations. Sequencing libraries were prepared from an equal number of RPF with the TruSeq Small RNA library preparation kit (Illumina). Next generation sequencing was performed using a HisEq. 2500 single read 75.

Bioinformatic analysis: From raw data to alignment files. Raw data were first trimmed to remove the 3′ adapter sequence with CutAdapt 1.9.1 configured with –e 0.12, -m 24, -M 35 (-M 51 for RNA-seq) and -a options to select a read size in a range from 24 to 35 nt allowing 12% of error. The trimmed reads were then mapped against the rRNA sequences of hg38 human genome with Bowtie 1.1.2 set up with –all and –un options. The –un option was used to select all unmapped reads. These filtered reads were finally mapped against the complete genome (hg38 human genome) and against the coding sequences only with Bowtie 1.1.2. The latter alignments were configured with two mismatches allowed (-n 2) and only uniquely mapped reads were selected (-m 1). The sam formatted files generated by the aligner were converted to sorted and indexed bam-formatted files using the Samtools program.

Differential expression. The number of reads for each gene was calculated with the featureCounts 1.5.0-p2 program and normalized with DESeq2 method through SARTools R Package. GO terms were identified for genes showing a significant expression variation using Panther (43). To represent RNA-seq and RIBO-seq profiles, we used the cross graphic representation where we display log_2 fold-changes in both data. The data were directly taken from the tables generated by SARTools. The colors were then selected based on the Panther groups and manually curated in case of no panther group was identified. The graphic was done using Bokeh v0.12.9 (https://bokeh.pydata.org/en/0.12.9/).

Ribosome footprints repartition. To identify reads as ribosome footprints, we did a metagene over the transcripts of hg38 human assembly to study the periodicity and the proportion of reads mapped on the CDS, UTR5, and UTR3. This analysis was done using only the 28 Mers, which are the most abundant kmers. Only transcripts coding for proteins with "appris_principal" tag were kept which represent 26,176 transcripts. For the metagene, we selected the 100 last nucleotides of the UTR5, the 100 first nucleotides of the UTR3 and the 100 first and 100 last nucleotides of the CDS. All transcripts that didn't have one of these three requirements was discarded for the metagene analysis. With these filters, we analyzed 25,062 CDS and 14,859 UTR5/3. From this metagene, we counted the proportion of mapped reads (28Mers) and realized a Fourier transform using the scipy package with the scipy.fft.fft function to study the periodicty. Python Bokeh library v0.12.9 was used to plot the percentages of mapped 28Mers on each feature and their corresponding period detected from Fourier transform results.

In vitro hybrid translation. Hybrid in vitro translation assay was performed as described previously (35) and is summarized hereafter. After centrifugation of 1 mL of RRL for 2 h 15 min at 240,000 × *g*, 900 μL of ribosome-free RRL (named S100) was collected, frozen, and stored at −80 °C. The extent of ribosome depletion from reticulocyte lysate was checked by translating 27 nM of in vitro transcribed capped and polyadenylated globin-*Renilla* mRNA in the S100 RRL and validated when no luciferase activity could be detected. In parallel, transfected cells were lysed in hypotonic buffer R [Hepes 10 mM pH 7.5, CH_3CO_2K 10 mM, $(CH_3CO_2)_2Mg$ 1 mM, DTT 1 mM] and potter homogenized (around 100 strokes). Cytoplasmic fraction was obtained by 13,000 × *g* centrifugation for 10 min at 4 °C. The ribosomal pellet was then obtained by ultracentrifugation for 2 h 15 min at 240,000 × *g* in a 1 M sucrose cushion and was rinsed three times in buffer R2 containing Hepes 20 mM, NaCl 10 mM, KCl 25 mM, $MgCl_2$ 1.1 mM, β-mercaptoethanol 7 mM and suspended in 30 μL of buffer R2 to reach more than 10 μg/μL ribosome concentration for optimal and long storage at −80 °C. The reconstituted lysate was then assembled by mixing 5 μL of S100 RRL with a scale from 0.25 to 4 μg of ribosomal pellet. Typically, the standard reaction contained 5 μL of ribosome-free RRL with 1 μg ribosomal pellet in a final volume of 10 μL. Upon reconstitution, the translation mixture was supplemented with 75 mM KCl, 0.75 mM $MgCl_2$, and 20 μM amino acid mix.

For in vitro translation assays, p0-*Renilla* vectors containing the β-globin, GAPDH 5′UTR, CrPV, DCV, or EMCV IRESs were described previously (38). mRNAs were obtained by in vitro transcription, using 1 μg of DNA templates linearized at the AflII sites, 20 U of T7 RNA polymerase (Promega), 40 U of RNAsin (promega), 1.6 mM of each ribonucleotide triphosphate, 3 mM DTT in transcription buffer containing 40 mM Tris·HCl (pH 7.9), 6 mM $MgCl_2$, 2 mM spermidine, and 10 mM NaCl. For capped mRNAs, the GTP concentration was reduced to 0.32 mM and 1.28 mM of m7GpppG cap analog (for β-globin mRNA) or m7GpppA (for CrPV mRNA) (New England Biolabs) was added. The transcription reaction was carried out at 37 °C for 2 h, the mixture was treated with DNase and the mRNAs were precipitated with ammonium acetate at a final concentration of 2.5 M. The mRNA pellet was then suspended in 30 μL of RNase-free water and mRNA concentration was determined by absorbance using the Nanodrop technology. mRNA integrity was checked by electrophoresis on nondenaturing agarose gel.

Statistical Analysis. Statistical analysis was performed using the Prism software (v7.0. GraphPad). A two-tailed Student *t* test was used for evaluating significance, except for RiboMethSeq data for which a one-tailed *t* test was used.

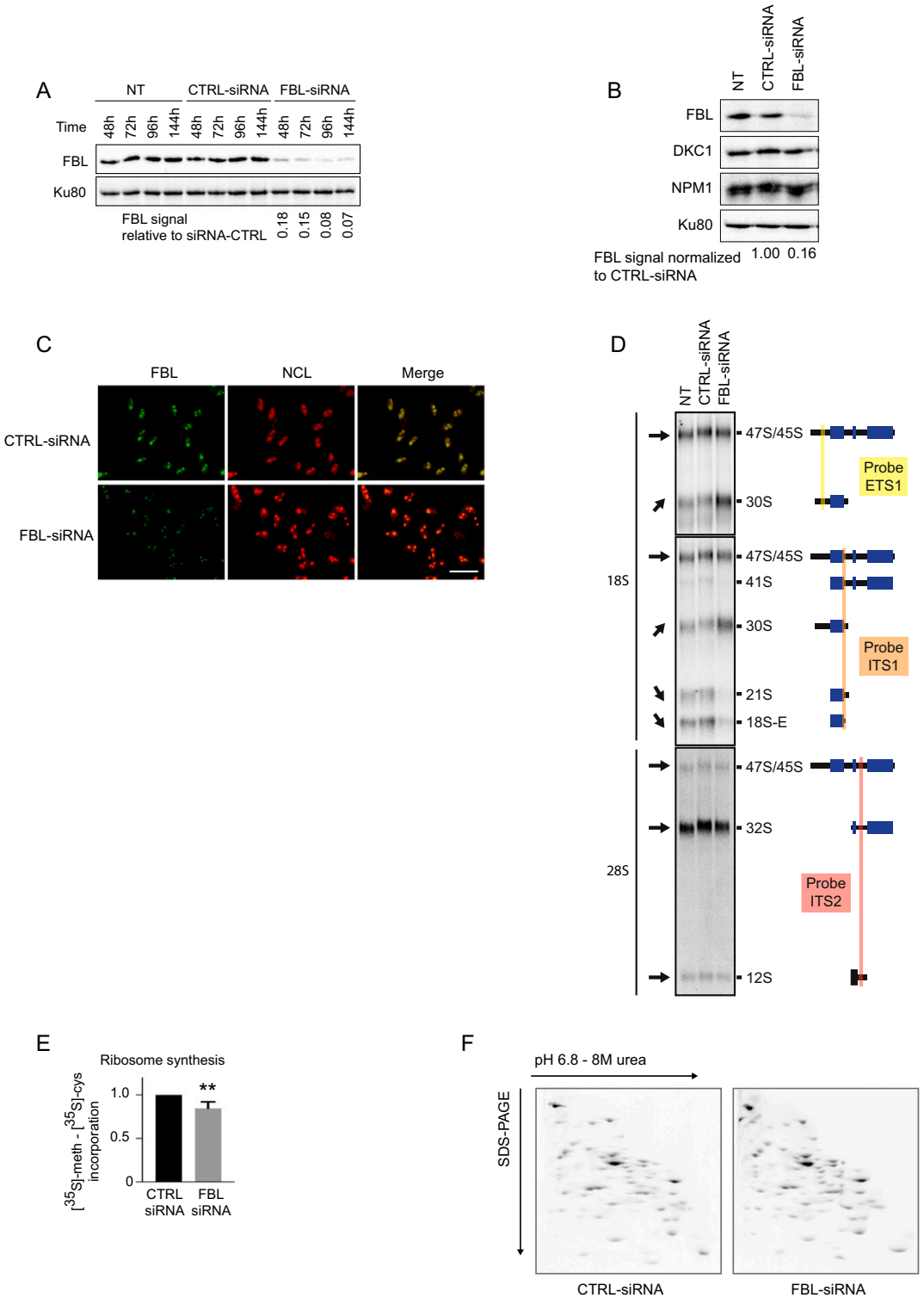

Fig. S1. Related to Fig. 1. Impact of FBL knockdown on major nucleolar markers. (*A*) Western blot analysis of *FBL* in HeLa cells transfected with three siRNAs targeting FBL for the periods of time indicated above each lane. Ku80 was used as a loading control. FBL signal was quantified and normalized against CTRL-siRNA (values are indicated below for each condition). (*B*) Western blot analysis of dyskerin (DKC1) and nucleophosmin (NMP1) levels in FBL knockdown HeLa cells compared with nontransfected cells (NT) and cells transfected with a CTRL-siRNA. Analysis performed 72 h posttransfection. Ku80 was used as a loading control. FBL signal was quantified and normalized against the CTRL-siRNA condition. (*C*) Immunofluorescence detection of FBL (green) and nucleolin (NCL) (red) 72 h after transfection with CTRL or FBL-siRNA. (Scale bar, 10 μm.) (*D*) Northern blot analysis of pre-rRNA processing in nontransfected (NT) or siRNA transfected (CTRL-siRNA and FBL-siRNA) HeLa cells. The position of the probes used and the detected prerRNA species are indicated on the right. Arrows on the left indicate the trend of each species in FBL-siRNA cells to increase or decrease compared with CTRL-siRNA cells. (*E*) Ribosome synthesis rate. [^{35}S]-Meth–[^{35}S]-Cys incorporation into purified cytoplasmic ribosomes 72 h after siRNA transfection in HeLa cells. Radioactivity was measured by liquid scintillation. Values are presented as mean ± SD ($n = 2$). **$P \leq 0.01$. (*F*) The 2D-PAGE analysis of 0.5 M KCl-purified ribosomes extracted from [^{35}S]-Meth–[^{35}S]-Cys pulse-labeled cells. Proteins were separated according to their charge in the first dimension and according to their molecular weight in the second dimension. Images show the radioactive signal obtained by phosphor-imaging.

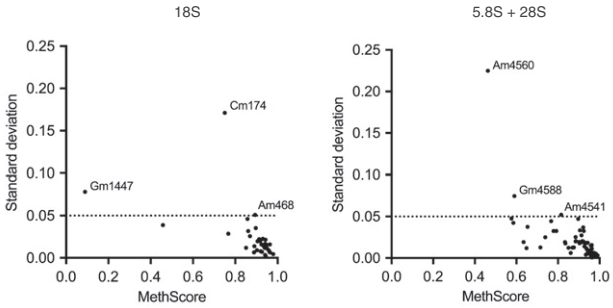

Fig. S2. Related to Fig. 2. Quantitative mapping of rRNA 2′-O-Me in human cells. Variability (SD) of RiboMethSeq data for each 2′-O-Me site, according to its level of methylation. Sites with variability greater than 5% are named on the graph. Most sites show a variability below 5% (dotted line). Values are represented as means of three independent biological replicates.

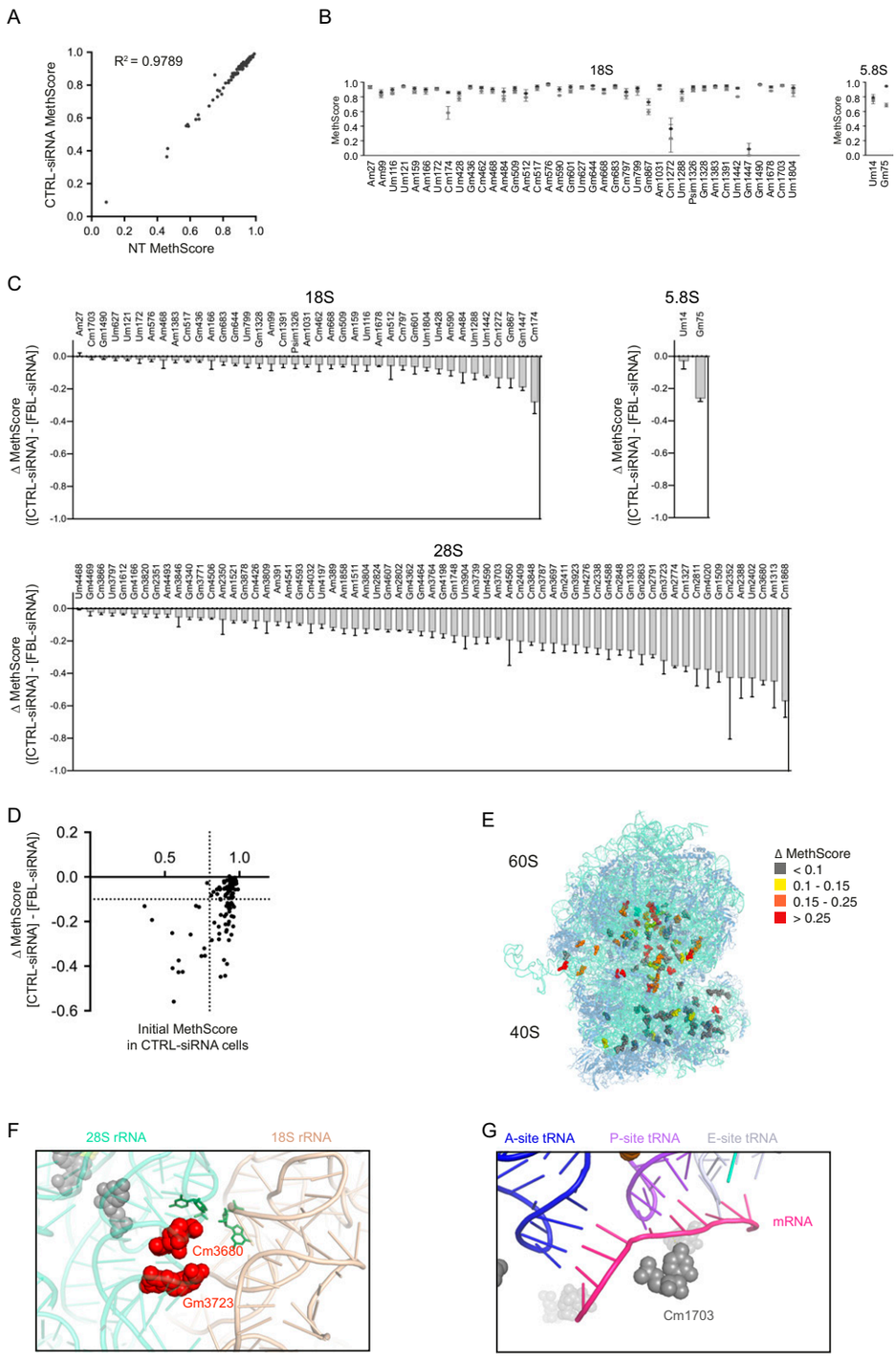

Fig. S3. Related to Fig. 3. Identification and localization of altered 2′-O-Me sites. (*A*) siRNA transfection has no effect on 2′-O-Me. Plot of the MethScore of each site in nontreated HeLa cells (NT) vs. HeLa cells transfected with control siRNA (CTRL-siRNA). Correlation coefficient (R2) was calculated from the linear regression curve. (*B*) Alteration of 2′-O-Me upon *FBL* knockdown. Mean MethScore values ± SD ($n = 3$ independent biological replicates) for each methylated nucleotide in 18S and 5.8S rRNA from HeLa cells transfected with CTRL-siRNA (black circle) or FBL-siRNA (gray circle). (*C*) FBL knockdown induces a decrease of MethScore at all but one site. For each site, the MethScore obtained in FBL-siRNA transfected HeLa cells was subtracted from the one from CTRL-siRNA transfected cells (same dataset as in Fig. 2*B*). Sites are shown in order of increasing difference in MethScore for the 18S, 5.8S, and 28S rRNAs. Error bars are SD from three independent biological replicates. (*D*) Distribution of 2′-O-Me sites according to their initial methylation frequency (*x* axis) and to their methylation variation upon FBL knockdown (*y* axis). Partially methylated sites in siRNA-CTRL cells (left of the vertical dotted line) were all down-methylated in siFBL-cells (ΔMethScore > 0.1). Note that the site 18S-Cm1447 was excluded, since it is not methylated our HeLa cells. (*E*) Position of methylated nucleotides on the 3D structure of the human ribosome, shown as assembled 80S ribosome. Nucleotides are color-coded according to the variation in MethScore comparing FBL-siRNA cells with CTRL-siRNA cells. See also Datasets S2 and S3. (*F*) View of intersubunit bridge B2b [18S-1051 and 28S-3699 (shown as stick in green)], showing close proximity of Cm3680 and Gm3723 methylation sites (red), which methylation was decreased by 44.3% and 32.0%, respectively. (*G*) View of the decoding center, showing the anticodon loop of tRNAs interacting with the mRNA at the A, P, and E-sites. The Cm1703 nucleotide (gray, not affected by FBL knockdown) is close to the mRNA.

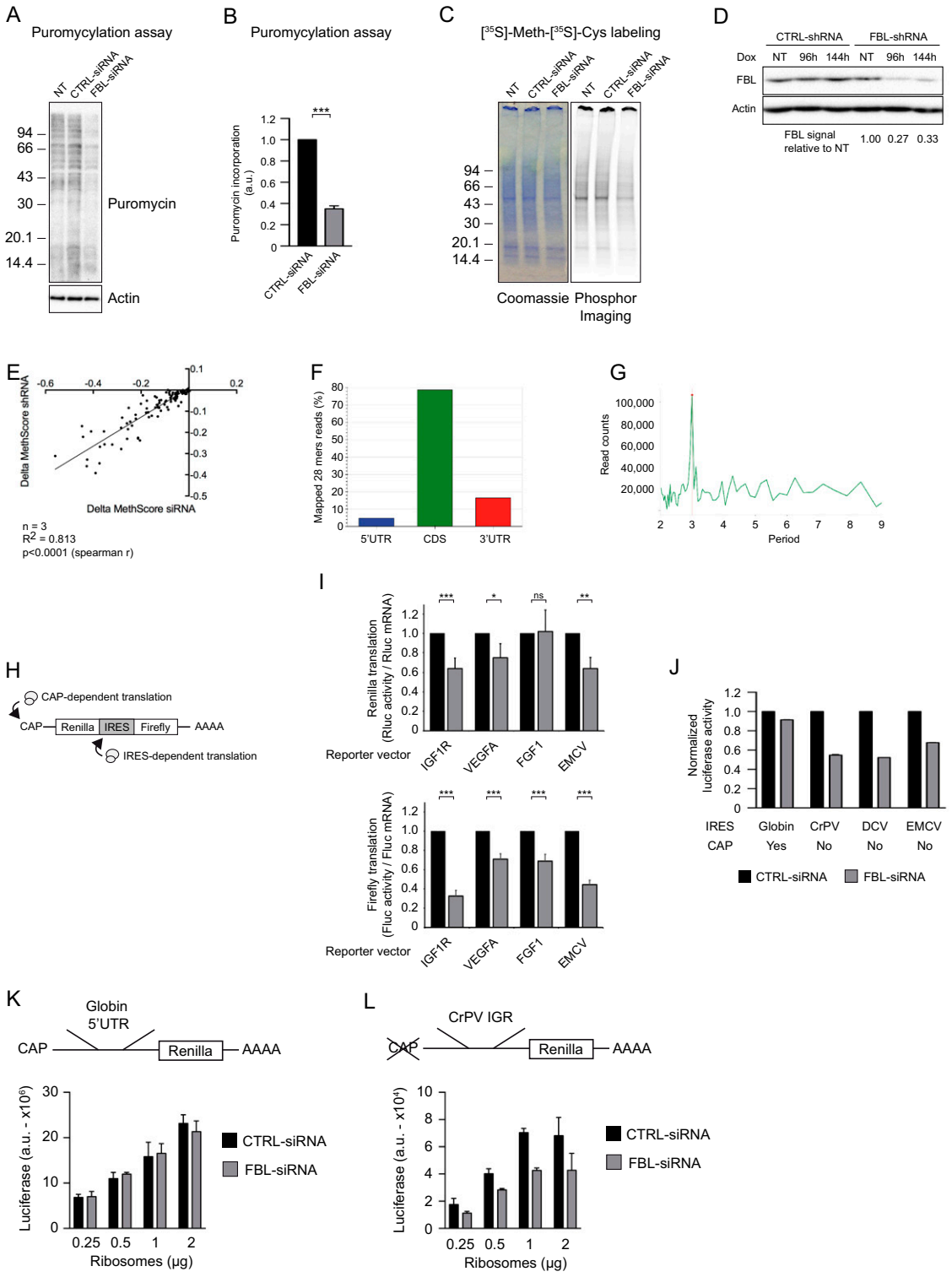

Fig. S4. Related to Fig. 4. rRNA methylation defect impairs IRES dependent translation from various viral IRES elements. (*A*) Global protein synthesis detection by incorporation of puromycin in nascent peptides. A representative Western blot with an antipuromycin antibody is shown. Actin detection was used as loading reference. (*B*) Global protein synthesis was measured by incorporation of puromycin in nascent peptides using Western blot against puromycin. Puromycin signal was normalized against actin. Values are presented as mean ± SD ($n = 3$). (*C*) Global protein synthesis detection by pulse labeling with [^{35}S]-methionine and [^{35}S]cysteine. A representative SDS/PAGE stained with Coomassie is shown (*Left*). The corresponding radioactive signal is shown upon phosphor-Imaging detection (*Right*). (*D*) Western blot analysis of *FBL* level in HeLa cells in which the expression of a CTRL shRNA or a FBL-shRNA was induced for 120 h by doxycycline (Dox) treatment. Actin was used as a loading control. The level of FBL upon shRNA expression is indicated below and normalized to CTRL-shRNA. (*E*) Plotting of the decrease of 2′-O-Me (ΔMethScore) in FBL-shRNA expressing cells (*y* axis) and of the ΔMethScore in FBL siRNA transfected cells (*x* axis). The data shows that the change in pattern of 2′-O-Me is similar in shRNA expressing cells compared with siRNA expression cells (Spearman *r* test, $P <$ 0.0001). (*F*) Fraction of the mapped 28Mers on each feature of transcripts. In this metagene, transcripts with a CDS length lower than 200 nucleotides and a 5′

Legend continued on following page

UTR and 3′UTR lengths lower than 100 nt were discarded. (*G*) Period detected from the frequencies of RPF obtained by fast Fourier transform. The red dot shows the most frequent period found in the data. The vertical red line shows the expected period of 3 nt for ribosome signals. This periodicity is not observed in UTRs regions indicating that the RPF correspond to active ribosome footprints. (*H*) Representation of in cellulo IRES-dependent translation assay using a bicistronic luciferase reporter construct. *Renilla* luciferase is translated in a Cap-dependent manner and Firefly luciferase is translated from the IRES element. (*I*) Translation efficiency of individual luciferase reporters was evaluated as the ratio of luciferase activity over mRNA levels. Luciferase activities were measured as in Fig. 4 and compared with luciferase mRNA levels measured by RT-qPCR. Data represent activity/mRNA ratios for Rluc (*Upper*, gray bars) and Fluc (*Lower*, gray bars), normalized against CTRL-siRNA (black bars). Values are presented as mean ± SD ($n = 3$). (*J*) Ribosomes purified from HeLa cells transfected with either CTRL-siRNA or FBL-siRNA were used to translate mRNAs in the hybrid in vitro translation assay. Translation was evaluated on luciferase reporter mRNAs containing a 5′UTR originating from human globin mRNA, or containing IRES elements from the CrPV, the DCV, or EMCV. The presence of Cap on the mRNA is indicated below the graph. Data are presented as mean ± SD ($n = 2$). (*K* and *L*) Identical experimental set-up as in Fig. 4*F* using a range of ribosome quantities. Data represent mean values (±SD, $n = 3$). Statistical significance was verified by conducting a Student *t* test. ns, not significant; $*P \leq 0.05$; $**P \leq 0.01$; $***P \leq 0.001$.

Other Supporting Information Files

Dataset S1 (XLSX)
Dataset S2 (XLSX)
Dataset S3 (XLSX)